The Molten Helix: Effects of Solvation on the α- to 3_{10}-Helical Transition

Mark L. Smythe,† Shawn E. Huston, and Garland R. Marshall*

Contribution from the Center for Molecular Design, Washington University, St. Louis, Missouri 63130-4899

Received August 24, 1994®

Abstract: Free energy surfaces, or potentials of mean force, for the α- to 3_{10}-helical conformational transition in polypeptides have been calculated in several solvents of different dielectric. The α- to 3_{10}-helical transition has been suggested as potentially important in various biological processes, including protein folding, formation of voltage-gated ion channels, kinetics of substrate binding in proteins, and signal transduction mechanisms. This study investigates the thermodynamics of the α- to 3_{10}-helical transition of a model peptide, the capped decamer of α-methylalanine, in order to assess the plausibility of this transition in the mechanisms of such biological processes. The free energy surfaces indicate that in each environment studied the α-helical conformation is the more stable of the two for the decapeptide. The thermodynamic data suggest that the α-helix is energetically stabilized and the 3_{10}-helix is entropically favored. The inclusion of dichloromethane, acetonitrile, or water results in approximately 7 kcal/mol of relative conformational energy (favoring the α-helix) and 3 kcal/mol of relative conformational entropy (favoring the 3_{10}-helix) in comparison to the gas phase. In polar environments, the α-helix is stabilized by its more favorable solute−solvent electrostatic interactions, and solute−solute steric interactions. In addition, it was concluded that in polar solvents, especially water, it is possible for the peptide to reduce some of the inherent strain of the 3_{10}-helix by widening ψ, the resulting weaker intrasolute hydrogen bonds being compensated for by increased hydrogen bonding to the solvent. Lower polarity environments are associated with a marginally increased relative stability of the 3_{10}-helix, which we suggest is largely due to the additional intrahelical hydrogen bond of this conformation. The data suggest that, in environments such as membranes, the interior of proteins or crystals, the complete transition from an α-helix to a 3_{10}-helix for this decapeptide would require less than 6 kcal/mol in free energy. Switching conformations for individual residues is much more facile, and shorter 3_{10}-helices may actually be energetically favored, at least, in nonpolar environments. This study primarily estimates the backbone contribution to the helical transition; side chain interactions would be expected to play a significant role in stabilizing one conformer relative to the other. It is, therefore, quite feasible that the α- to 3_{10}-helical transition could provide a possible mechanism for many biological processes. While there are many factors, such as helix length and side chain packing, that contribute to the selection of either the α- or the 3_{10}-helical conformation or a mixture of the two, this study focuses primarily on one of these effects, that of the polarity of the environment.

Introduction

The α-helix, first proposed as a model structure by Pauling *et al.*,[1] is a well-known and quite common secondary structure element in proteins. The 3_{10}-helix, described by Taylor *et al.*[2] and proposed in detail by Donahue,[3] accounts for 10% of helical residues in proteins.[4] These 3_{10}-helices are usually short, about 4 residues in length, though 3_{10}-helices of 7−12 residues in length have been reported in proteins.[5,6] Whereas the α-helix is characterized by a $[i, i + 4]$, thirteen-membered, hydrogen-bonding pattern, where the notation $[i, i + 4]$ designates a hydrogen bond between the carbonyl oxygen atom of residue i and the amide hydrogen of residue $i + 4$, the 3_{10}-helix is distinguished by an $[i, i + 3]$, ten-membered, hydrogen-bonding arrangement.

Both α- and 3_{10}-helices are common features in the crystal structures of smaller peptides containing a mixture of α-monoalkyl and α,α-dialkyl amino acids. The most predominant α,α-dialky amino acid found in such peptides is α-methylalanine (MeA; aminoisobutyric acid, Aib). The conformational properties of MeA are significantly different from those of α-monoalkyl amino acids. The MeA residue is severely conformationally restricted and populates almost exclusively right- and left-handed helical conformations.[7] Consequently, the numerous crystal structures of peptides containing MeA residues are invariably either α- or 3_{10}-helical, or some mixture of the two. The sensitivity of the preferential formation of either an α- or 3_{10}-helix to a host of factors[11] is illustrated by, for example, crystallographic data that show sensitivity to protecting group (Ac vs Boc) and solvent of crystallization.[8] Indeed, both helical types have been observed in the same crystal.[8] There is crystal structure evidence for α- to 3_{10}-helical transitions in enzymes occurring as a result of substrate binding to lactate dehydrogenase[9] and to mitochondrial aminotransferase.[10] Due to these observations, and the role of peptides containing MeA (such as the peptaibol antibiotics[11]) in causing voltage-dependent conductance in membranes, there has been a great deal of interest

† Current Address: Centre for Drug Design and Development, The University of Queensland, Brisbane QLD 4072. Australia.

® Abstract published in *Advance ACS Abstracts*, May 1, 1995.

(1) Pauling, L.; Corey, R. B.; Branson, H. R. *Proc. Natl. Acad. Sci. U.S.A.* **1951**, *37*, 205−211.
(2) Taylor, H. S. *Proc. Am. Phil. Soc.* **1941**, *85*, 1−7.
(3) Donohue, J. *Proc. Natl. Acad. Sci. U.S.A.* **1953**, *39*, 470−478.
(4) Barlow, D. J.; Thornton, J. M. *J. Mol. Biol.* **1988**, *201*, 601−619.
(5) Robbins, D. J.; Stout, C. D. *Proteins: Struct., Funct. Genet.* **1989**, *5*, 289−312.
(6) Pathak, D.; Ollis, D. *J. Mol. Biol.* **1990**, *214*, 497−525.
(7) Marshall, G. R.; Bosshard, H. E. *Circ. Res Suppl. II* **1972**, *30/31*, 143−150.
(8) Karle, I. L.; Balaram, P. *Biochemistry* **1990**, *29*, 6747−56.
(9) Gerstein, M.; Chothia, C. *J. Mol. Biol* **1991**, *220*, 133−149.
(10) McPhalen, C. A.; Vincent, M. G.; Picot, D.; Jansonius, J. N.; Lesk, A. M.; Chothia, C. *J. Mol. Biol.* **1992**, *227*, 197−213.

0002-7863/95/1517-5445$09.00/0

in trying to understand the preferences for α- or 3_{10}-helical conformations and the transition between these two states.[12-18]

The majority of these studies investigate the helical transition for oligomers of MeA. MeA oligomers are commonly used due to the possible mechanistic importance of the α- to 3_{10}-helical transition of peptaibols in ion-channel formation and the conformational properties of this residue. It is of interest to better understand the conformational equilibrium not only in MeA-derived peptides but also in peptides composed of α-monoalkylated residues. The results presented here will be used as the basis for future work targeted at understanding the interhelical conversion involving these latter amino acids as well.

Previously, we have reported[12] preliminary potential of mean force (pmf) calculations of the α- to 3_{10}-helical transition of Ac−$(MeA)_{10}$−NMe in water and acetonitrile (CH_3CN) and *in vacuo*. Here, we report more detailed thermodynamic and structural results of the α- to 3_{10}-helical transition in these environments, as well as additional data on the helical transition in methylene chloride (CH_2Cl_2).

Experimental Section

Potentials of Mean Force. The potential of mean force as a function of a coordinate ξ is $W(\xi) = -kT \ln(p(\xi))$, where k is Boltzmann's constant, T is the absolute temperature, and $p(\xi)$ is the probability density along that coordinate. Because ordinary molecular dynamics simulations are limited to nanosecond time scales, it is difficult to guarantee adequate sampling of conformational space in the regions of high potential barriers. It is possible, however, to introduce modified dynamical methods for which adequate sampling of these high-energy regions can be obtained. One such approach, the umbrella sampling technique,[19-21] was used here to determine $p(\xi)$. Umbrella sampling uses an auxiliary "window" potential $U(\xi)$ to improve the uniformity of the sampling along ξ. Systematically shifting the minimum of $U(\xi)$ along the coordinate ξ results in sampling conformations in a series of overlapping windows (simulations) that are centered around different values of ξ. The resulting potential of mean force W^* is then given by $W^*(\xi) = W(\xi) + U(\xi) + C$ and is related to the probability density p^* (that probability calculated in the presence of the umbrella potential) by $W^*(\xi) = -kT \ln (p^*(\xi))$.[22] The constants C are different for each window and are calculated by requiring that $W(\xi)$ be a continuous function of ξ and by arbitrarily selecting the zero of the free energy $W(\xi^\circ) = 0$.[19,22]

The reaction coordinate used by this transition has been previously determined,[13,16] and it is well-approximated by a linear change of the peptide end-to-end distance. Furthermore, while this manuscript was in preparation, Basu *et al.*[23] analyzed a 2-ns molecular dynamics simulation of MeA_8 by principal component analysis and showed that the first principal component which accounted for 61.5% of the total fluctuation of the peptide correlated with the linear end-to-end distance. Therefore, this distance, denoted by $r^{\alpha\alpha}$ and defined as the distance from the α-carbon of the first residue to the α-carbon of the last residue, was used as the reaction coordinate for the calculation of the pmf's. For the MeA decamer, this involved simulations centered on $r^{\alpha\alpha} = 13$ Å to $r^{\alpha\alpha} = 19$ Å in 1-Å increments.

Entropy Calculation. Use of expression 1 derived by Huston and Marshall[13] has allowed us to calculate the entropic profile for the transitions.

$$-T\delta S(r) = \Delta A(r) - \frac{kT^2}{2\Delta T} \ln\left[\frac{\langle w_+ \delta(r' - r)\rangle_r}{\langle w_- \delta(r' - r)\rangle_r}\right] + C_s \quad (1)$$

In eq 1, $\Delta A(r)$ is the potential of mean force, corrected to remove the effects of the auxiliary potential, $w_\pm = \exp[-(U/k)T_\pm]$, U is the potential energy, $T_\pm = 1/(T \pm \Delta T) - 1/T$, and $\langle w_\pm \delta(r' - r)\rangle_T$ is calculated from the simulation carried out at temperature T. The unknown additive constant in the entropy calculation (C_s) is accounted for in the same manner as for the pmf calculations.[13] A temperature-perturbation step size ΔT of 2° is used here; however, choosing $\Delta T = 5°$ did not alter the results. This method is not numerically equivalent to the direct calculation of $\langle U \rangle$ as it's estimated error is much less.

Details of Simulations. Four series of simulations were conducted, in the gas phase, CH_3CN, CH_2Cl_2, and water. The peptide studied (CH_3CO−MeA_{10}−NMe) was represented by the AMBER/OPLS force field.[20,21] This force field which utilized a united atom description of CH_n groups is commonly used and has been shown to provide a good description of the conformational energetics of alanine[24,25] and the hydration free energies of small organic compounds.[26] The OPLS solvent models have been developed to accurately reproduce experimental properties of liquids and are known to reasonably reproduce the structural properties of solvent.[21] The TIP3P model for water,[27] published parameters for CH_3CN,[28] and unpublished CH_2Cl_2 parameters provided by W. Jorgensen and colleagues were used for the explicit solvent simulations.

The initial 3_{10}- and α-helical conformations were model built using the SYBYL software from Tripos Associates.[29] To generate the solvated peptide systems, a 3_{10}-helix was centered in a rectangular box of equilibrated solvent molecules. Any solvent molecules with oxygen-to-solute or hydrogen-to-solute distances less then 2.8 or 2.0 Å, respectively, or farther than 8.0 Å from the closest peptide atom in any one Cartesian direction were deleted. For the aqueous system, the simulation cell contained the solute plus 467 water molecules in a box of dimensions 36.86 × 21.97 × 22.14 Å^3. The system comprised 335 CH_3CN molecules in a box of dimensions 40.69 × 28.26 × 28.26 Å^3 for the CH_3CN solvent and 316 solvent molecules in a box of dimensions 43.76 × 27.87 × 28.30 Å^3 for CH_2Cl_2. Prior to equilibrating any prepared system, it was subject to the following 4-step minimization protocol. First, only the solute was minimized, then only the solvent was minimized, and this was followed by minimization of the entire system. Finally, the whole system was again minimized, this time using SHAKE[30] for a further 500 cycles of conjugate gradient minimizations. In all cases, the helical axes of the peptide did not shift significantly relative to the rectangular coordinates of the simulation cells during the simulations, thus maintaining correct solvation.

All simulations were carried out at 298 K with periodic boundary conditions and were conducted on IBM risc/6000 workstations using

(11) Marshall, G. R.; Beusen, D. D. In *Biomembrane Electrochemistry*; Blank, M., Vodyanoy, I., Eds.; American Chemical Society: Washington, DC, 1994; Adv. Chem. Ser. No. 235, pp 259−314.
(12) Smythe, M. L.; Huston, S. E.; Marshall, G. R. *J. Am. Chem. Soc.* **1993**, *115*, 11594−11595.
(13) Huston, S. E.; Marshall, G. R. *Biopolymers* **1994**, *34*, 75−90.
(14) Marshall, G. R.; Hodgkin, E. E.; Langs, D. A.; Smith, G. D.; Zabrocki, J.; Leplawy, M. T. *Proc. Natl. Acad. Sci. U.S.A.* **1990**, *87*, 487−91.
(15) Aleman, C.; Subirana, J. A.; Perez, J. J. *Biopolymers* **1992**, *32*, 621−631.
(16) Clark, J. D.; Hodgkin, E. E.; Marshall, G. R. In *Molecular Conformation and Biological Interactions (Prof. G. N. Ramachandran Festschrift)*; Balaram, P., Ramaseshan, S., Eds.; Indian Academy of Sciences: Bangalore, India, 1991; pp 503−510.
(17) Hodgkin, E. E.; Clark, J. D.; Miller, K. R.; Marshall, G. R. *Biopolymers* **1990**, *30*, 533−546.
(18) Aleman, C.; Perez, J. J. *Int. J. Quant. Chem.* **1993**, *47*, 231−238.
(19) Valleau, J. P.; Torrie, G. M. In *Statistical Mechanics, Part A*; Berne, B. J., Ed.; Plenum: New York, 1977; Chapter 5.
(20) Weiner, S. J.; Kollman, P. A.; Case, D. A.; Singh, U. C.; Ghio, C.; Alagona, G.; Profeta, S.; Weiner, P. J. *J. Am. Chem. Soc.*, **1984**, *106*, 765−784.
(21) Jorgensen, W. L.; Tirado-Rives, J. *J. Am. Chem. Soc.* **1988**, *110*, 1657−1666.
(22) Northrup, S. H.; Pear, M. R.; Lee, C.-Y.; McCammon, J. A.; Karplus, M. *Biochemistry* **1982**, *79*, 4035−4039.
(23) Basu, G.; Kitao, A.; Hirata, F.; Go, N. *J. Am. Chem. Soc.* **1994**, *116*, 6307−6315.
(24) Tirado-Rives, J.; Maxwell, D. S.; Jorgensen, W. L. *J. Am. Chem. Soc.* **1993**, *115*, 11590−11593.
(25) Brooks, C. L.; Case, D. A. *Chem. Rev.* **1993**, *93*, 2487−2502.
(26) Czerminski, R.; Elber, R. *J. Chem. Phys.* **1990**, *92*, 5580−5601.
(27) Jorgensen, W. L.; Chandrasekhar, J.; Madura, J. D.; Impey, R. W.; Klein, M. L. *J. Chem. Phys.* **1983**, *79*, 926−935.
(28) Jorgensen, W. L.; Briggs, J. M. *Mol. Phys.* **1988**, *63*, 547−558.
(29) SYBYL, Tripos Associates Inc.: St. Louis, Missouri.
(30) Ryckaert, J. P.; Ciccotti, G.; Berendsen, H. J. C. *J. Comput. Phys.* **1977**, *23*, 327−341.

the AMBER 4.0 software,[31] with modifications to improve its use for umbrella sampling and to fix problems with periodic boundary conditions when using long bond constraints. The simulations used a 2-fs time step and coordinates were saved every 25 steps (50 fs) for further analysis. In the gas phase simulations, no nonbonded cutoff was used, while the explicit solvent simulations used a nonbonded pair list, generated using an 8.0-Å cutoff and updated every 25 steps. Seven overlapping windows were used, with a force constant of 5.0 (kcal mol^{-1}) $Å^2$ in the gas phase and 3.0 (kcal mol^{-1}) $Å^2$ in the solution simulations. A smooth conformational transfer between windows was found on examination of Ramachandran maps (Φ,Ψ) of the overlap regions between adjacent windows (data not shown). For the gas phase simulations, a total of 900 ps was run in each window, and for the explicit solvent simulations, 400 ps of molecular dynamics was generated in each window. The first 20 ps of any window's trajectory was taken as the equilibration period and discarded from the subsequent averages. Statistical uncertainties were calculated according to the method of block averages.

Two series of simulations were run in the gas phase and in CH_3CN, one each in the forward (α to 3_{10}) and reverse (3_{10} to α) directions. In the case of the forward direction, the simulation was started from the α-helical conformation, $r_o^{\alpha\alpha}$ = 14 Å. To generate the starting conformation for the $r_o^{\alpha\alpha}$ = 15 Å window, a conformation from the 14 Å window was selected and minimized with the 15 Å restraint in place. In this fashion, the reaction coordinate was "walked" from the α- to the 3_{10}-helix or *vice versa*.

As a further check on the extent of convergence of the pmfs, additional gas phase simulations for the 14-Å window were conducted. For this calculation, independent simulation cells were generated from simulations at the higher temperature of 400 K. Specifically, two of these higher temperature runs were performed, with the two previously generated 14-Å windows (one apiece from each of the forward and reverse directions) providing the initial configurations. Selection of three conformations from each of these higher temperature runs along with the two starting conformations provided a total of eight boxes, which were each simulated for 100 ps at 298 K.

A β-release of program CARNAL[32] (a general analysis package for use with the Amber suite of programs[31]) was used to analyze the molecular dynamics trajectory in addition to other programs written to analyze hydrogen bonds, surface areas,[33] and dipoles.

Results

In this section, we present our results for the free energy surfaces, as well as various derived thermodynamic quantities. We also report results from various analyses that have been used to characterize the conformations of the "end points" of the transition. The end points are defined as the conformations that are sampled within the α- and 3_{10}-helical regions of the pmf.

The free-energy surfaces obtained in the four environments are shown in Figure 1. The reference for all thermodynamic quantities is the free-energy minima of the α-helical state. In all four environments studied, the α-helix is the favored conformation for the decapeptide. The surfaces predict that in vacuum the α-3_{10} free-energy difference is dramatically different than in any of the solvents considered. In solution, the α-helix becomes increasingly stabilized with respect to increasing dielectric; up to a point, CH_3CN and water yield identical conformational free-energy differences.

The free-energy surface for the helical transition in CH_3CN has been calculated in the forward and reverse directions; these are displayed in Figure 2 and emphasize the high degree of reproducibility of the calculations. Figure 3 shows the free-energy surfaces resulting from the first half (20−200 ps) and the last half of the forward direction simulation (200−400 ps) of the conformational transition in CH_3CN. These data illustrate that the free-energy surface converges in the first 200 ps.

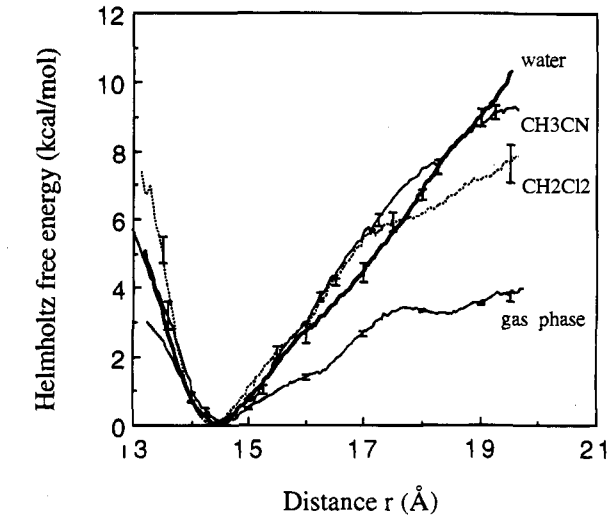

Figure 1. Computed potentials of mean force for the α- to 3_{10}-helical transition in various solvents. Statistical uncertainties were calculated according to the method of block averages.

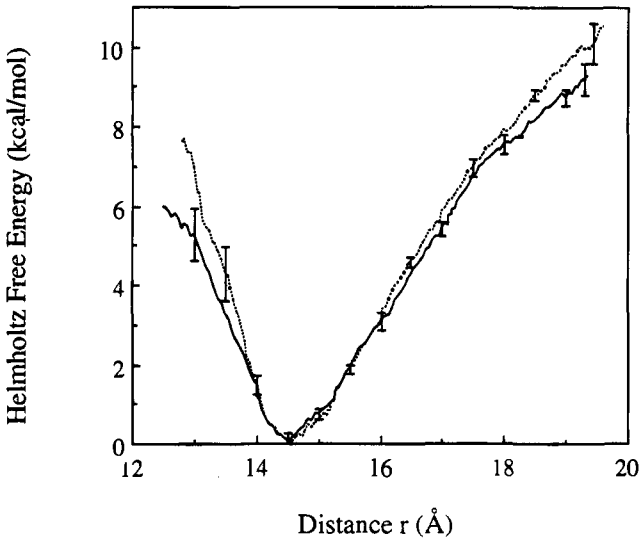

Figure 2. Computed potentials of mean force (forward and reverse direction) for the α- to 3_{10}-helical transition in acetonitrile. Statistical uncertainties were calculated according to the method of block averages.

One must uniformly sample the conformational space of the peptide in order to obtain a realistic estimate of the probability density along the reaction coordinate ($p(\zeta)$). In order to obtain an estimate of the conformational sampling of our molecular dynamics simulations, we have implemented the nonbonded force metric ($d_{FN}(t)$) of Straub and Thirumalai.[34,35] The nonbonded force metric is the root mean square of the atom-wise time-average nonbonded forces for two independent simulations;[34,35] the two independent simulations correspond to the forward and reverse directions in our case. Therefore, if both simulations broadly sample the same conformational space (and, thereby, sample common space), the average force on the molecule in the distinct simulations should become similar and $d_{FN}(t)$ should approach zero.

(31) Pearlman, D. A.; Case, D. A.; Caldwell, J. C.; Seibel, G. L.; Singh, U. C.; Weiner, P.; Kollman, P., AMBER 4.0; University of California, San Francisco.

(32) Ross, W. S., CARNAL (β-release); Department of Pharmaceutical Chemistry, UCSF, San Francisco, CA.

(33) Le Grand, S. M.; Merz, K. M., Jr. *J. Comp. Chem* **1993**, *14*, 349−352.

(34) Straub, J. E.; Thirumalai, D. *Proc. Natl. Acad. Sci. U.S.A.* **1993**, *90*, 809−183.

(35) Straub, J. E.; Thirumalai, D. *Proteins: Struct., Funct., Genet.* **1993**, *15*, 360−373.

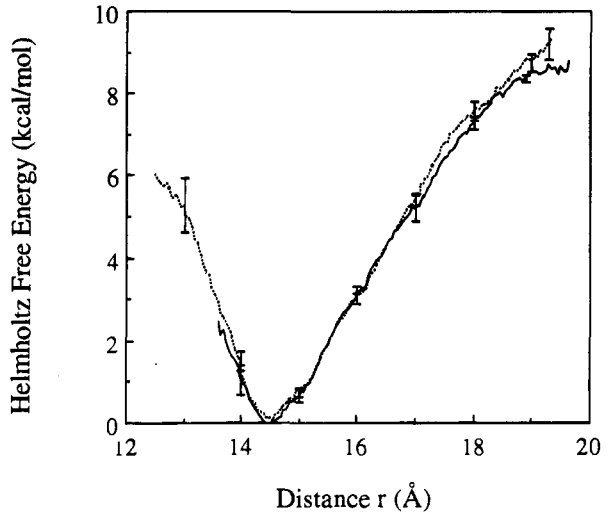

Figure 3. Computed potentials of mean force (20−200 ps, 200−400 ps) for the α- to 3_{10}-helical transition in acetonitrile. Statistical uncertainties were calculated according to the method of block averages.

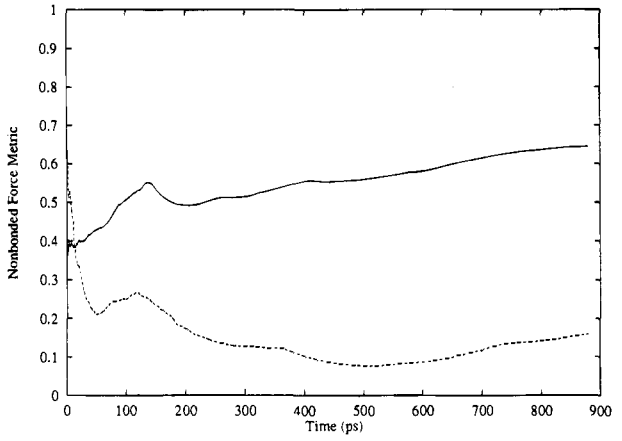

Figure 4. Plots of the nonbonded force metric[34,35] [$d_{FN}(t)/d_{FN}(0)$] as a function of time [$d_{FN}(0)$ denotes the initial ($t = 0$) value of this metric]. The solid line represents the $r^{\alpha\alpha} = 14$ Å window and the dashed line the $r^{\alpha\alpha} = 18$ Å window for the gas phase simulation.

The data in Figure 4 summarize the force metric calculations for the gas phase. In the case of the 18-Å window, it can be concluded that the two independent simulations are sampling the same conformational space. For the case of the 14-Å window, the two trajectories are seen to reside in separate conformational substates; this is clear from the large and persistent difference in nonbonded forces of the forward and reverse simulations (the rms difference in the average coordinates for the two simulations is 0.3 Å); transitions between these substates occur on a much longer time scale than explored by our simulations. This restriction in conformational sampling can be overcome by performing multiple simulations of moderate length from different starting conformations, rather than a single long simulation (see Experimental Section); the force metric data resulting from eight independent simulations conducted in this manner are shown in Figure 5. A dramatic difference in the behavior of $d_{FN}(t)$ compared with Figure 4 is seen (the rms difference in the average coordinates for the two data sets is now 0.04 Å). The multiple simulation method leads, not surprisingly, to much more effective sampling of conformational space. In fact, just the sort of seemingly unsatisfactory sampling results obtained here from the single long simulation protocol have prompted the development of newer, highly efficient simulation methods.[36] Interestingly, the improvement in conformational sampling has no effect on the calculated free-

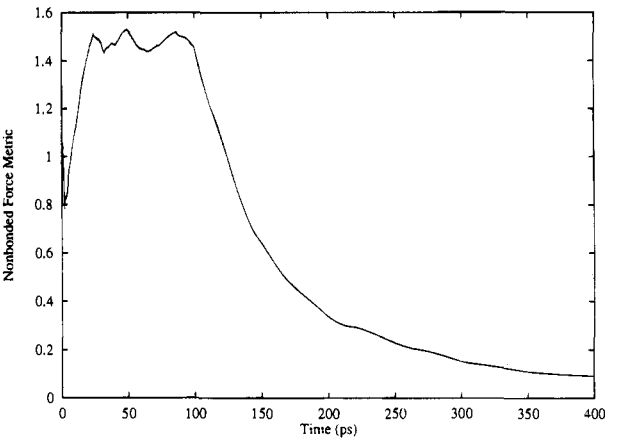

Figure 5. Plots of the nonbonded force metric[34,35] [$d_{FN}(t)/d_{FN}(0)$] as a function of time [$d_{FN}(0)$ is as described in Figure 4]. Conformational sampling was achieved by eight 100-ps simulations at $r^{\alpha\alpha} = 14$ Å. Starting configurations were selected at various intervals of a 400 K simulation ($r^{\alpha\alpha} = 14$ Å).

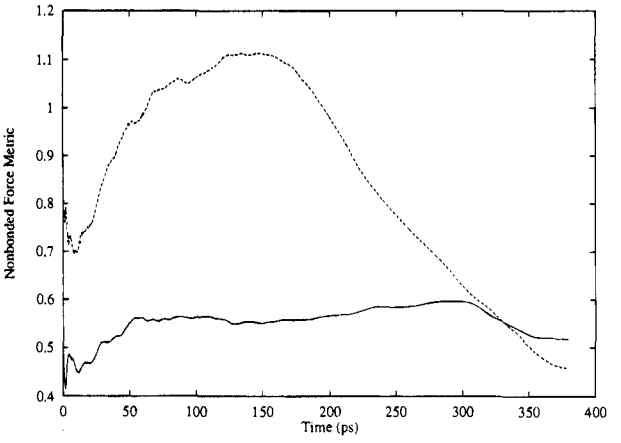

Figure 6. Plots of the nonbonded force metric[34,35] [$d_{FN}(t)/d_{FN}(0)$] as a function of time [$d_{FN}(0)$ is as described in Figure 4]. The solid line represents the $r^{\alpha\alpha} = 14$ Å window and the dashed lines the $r^{\alpha\alpha} = 18$ Å window for the CH_3CN simulation.

energy surface in this case. Apparently, the newly sampled conformational substates do not change the energetic distribution of conformers with respect to $r^{\alpha\alpha}$ for $r^{\alpha\alpha}$ near 14 Å. Previous studies have addressed the precision of various free-energy calculations.[37−39]

The data for the $r^{\alpha\alpha} = 14$ and 18 Å windows in CH_3CN are shown in Figure 6. The data illustrate that, in each case, the two independent trajectories are initially sampling different conformational substates, but the trajectories begin to mix after a time, as the barriers between the conformational substates are overcome. It can be seen that in the alloted simulation time the nonbonded force metric in CH_3CN decays less, with respect to its initial value, than was the case for the gas phase peptide. At the end of the simulation period, there is a residual component to the force metric, and additional time would further decrease this measure. However, given the lengthy nature of these solution phase simulations and the negligible effect additional sampling had on the gas phase pmf, we have chosen not to continue these simulations, as this would most likely only serve to fine tune the present results.

(36) Simmerling, C.; Elber, R. *J. Am. Chem. Soc.* **1994**, *116*, 2534−2547.
(37) Hermans, J.; Yun, R. H.; Anderson, A. G. *J. Comput. Chem.* **1992**, *13*, 429−442.
(38) Mitchell, M. J.; McCammon, J. A. *J. Comp. Chem.* **1991**, *12*, 271−275.
(39) Mazor, M.; Pettitt, B. M. *Mol. Simul.* **1991**, *6*, 1−4.

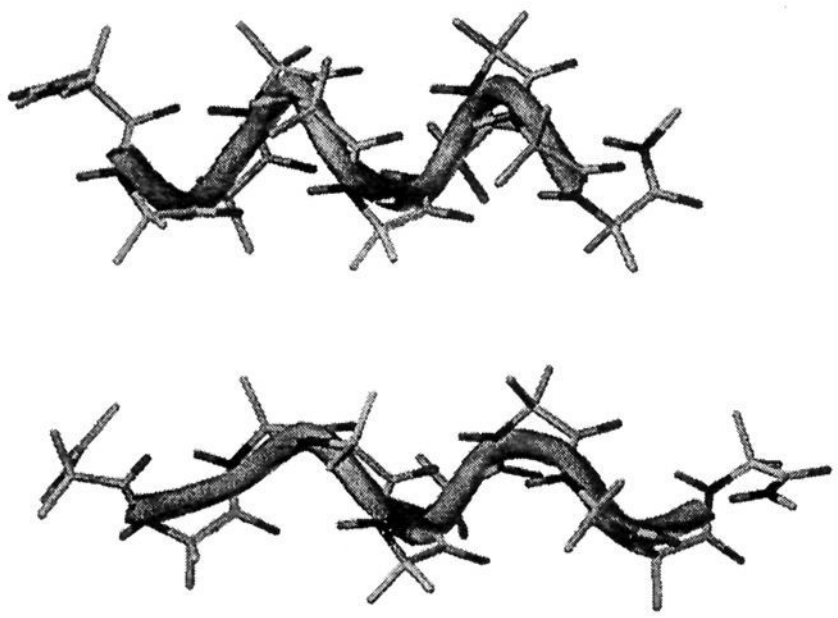

Figure 7. Average conformations of the α- and 3_{10}-helical end points in water.

Table 1. Mean Calculated ϕ,ψ Torsion Angles of Four Central Residues

	α-helix		3_{10}-helix	
	ϕ	ψ	ϕ	ψ
gas phase	-59.0 ± 8.3	-50.4 ± 7.8	-56.6 ± 11.0	-25.9 ± 15.2
CH_2Cl_2	-58.6 ± 7.7	-50.3 ± 7.4	-56.5 ± 10.7	-27.9 ± 12.8
CH_3CN	-59.4 ± 10.1	-49.3 ± 8.8	-59.5 ± 12.3	-31.9 ± 20.4
water	-59.5 ± 7.8	-50.3 ± 7.3	-58.8 ± 7.3	-37.9 ± 17.8

The measures described above indicate that the pmf's are reasonably well-converged and reproducible, and at this point, we turn to a more thorough discussion of the results obtained. The end points of the transitions have been characterized by a hydrogen bond and torsion angle analysis. In each simulation, the conformations of the end points show the expected helical character. Shown in Figure 7 are the average conformations of the α- and 3_{10}-helices in water. Average ϕ and ψ torsion angles of the central four residues of the end point conformations are given in Table 1. The first three and last three residues were omitted due to fraying of the helical termini. The average ϕ and ψ values from crystallographic data of MeA residues are -57 and $-50°$, respectively,[11] in α-helical peptides and -54 and $-28°$, respectively, in 3_{10}-helical peptides.[40] These values compare favorably with the data in Table 1, being matched most closely by the data from CH_2Cl_2 which has a low dielectric most comparable to those estimated for organic crystals. Most notable about the data in Table 1 is the large fluctuations of the ψ torsion of the 3_{10}-helical conformation in solvent and that this angle rotates substantially as the dielectric of the medium increases.

What role does this widening of ψ have on the peptide hydrogen bonds? The data in Table 2 show the average hydrogen-bond geometries of the central helical residues in each simulation. The data show that the hydrogen-bond geometry of the α-helical conformations is more favorable than that of the 3_{10}-helical conformations and is constant across all environments. In contrast, the geometry of the 3_{10}-helical hydrogen bonds gradually gets worse as the polarity of the environment increases. This is compensated by more hydrogen-bonding interactions with the solvent (see below and Figure 4).

The conformational free-energy difference between the α- and 3_{10}-helices in the various environments has been broken up into its energetic and entropic components according to $\Delta A = \Delta E - T\Delta S$ and eq 1. The data are given in Table 3. The differences in free energy between the two states show that going from gas phase CH_2Cl_2 or CH_3CN to water results in an increase in α-helical stability relative to the 3_{10}-helix. If we consider the energetic and entropic data (Table 3), the following conclusions can be made. Since all simulations show entropy favors the 3_{10}-helix, the overall thermodynamic instability of the 3_{10}-helix is energetically driven. It can be noted that simple normal mode analysis of the α and 3_{10} conformational minima yield concurring results as to the greater entropy of the 3_{10}-helix.[23] The data in Table 3 also illustrate that the magnitude of the energetic destabilization of the 3_{10}-helix is the same for each solvent. The same can be said for the entropic stabilization of the 3_{10}-helix, considering the large associated error. Thus, inclusion of solvent results in a further 7 kcal/mol of relative conformational energy (favoring the α-helix), and approximately 3 kcal/mol relative conformational entropy (favoring the 3_{10}-helix).

What drives this solvent-enhanced energetic destabilization of the 3_{10}-helical conformation? From examination of the solute−solute and solute−solvent components of the energy shown in Table 4, the following conclusions can only be suggested due to the large variation in results based on energy-entropy decompositions. The solute−solute electrostatic energy ($\Delta E_{\text{uu-el}}$) and the solute−solvent van der Waals energy ($\Delta E_{\text{uv-vdw}}$) favor the formation of the 3_{10}-helix. Therefore, the instability of the 3_{10}-helix is due to a combination of the solute−solute van der Waals ($\Delta E_{\text{uu-vdw}}$) and solute−solvent electrostatic ($\Delta E_{\text{uv-el}}$) components. The unfavorable intramolecular van der Waals energy of the 3_{10}-helix is well-documented[16,17] and accounts for the solute−solute van der Waals effect. The reason the $\Delta E_{\text{uv-el}}$ term favors the α-helix is primarily due to the additional solvent exposed amide hydrogen and carbonyl of this conformation with respect to the 3_{10}-helix. In addition, the average calculated dipole moments of the end point conformations (Table 5) illustrate the greater dipole moment of the α-helical conformation. These effects would result in a more favorable peptide−solvent electrostatic interaction energy for the α-helix, as observed. Furthermore, these factors would lead to a more favorable entropy for the 3_{10}-helix conformation, simply because fewer solvent molecules would be "bound" to this conformation. This trend is seen in the data, that is, a positive change in energy and a negative change in entropy in going from the α- to 3_{10}-helix.

In conclusion, the intramolecular van der Waals energy of the α-helix and the more favorable electrostatic interaction of this conformation with the solvent underlie its observed thermodynamic stability. For what reasons does the 3_{10}-helix become less thermodynamically stable in polar environments? In order to answer this question, we need to further investigate the data in Table 4. The data in Table 4 also illustrate that the $\Delta E_{\text{uv-vdw}}$ term is 4 kcal/mol more positive for water than for CH_2Cl_2 and CH_3CN. The $\Delta E_{\text{uv-vdw}}$ term favors the 3_{10}-helix in CH_2Cl_2 and CH_3CN partly due to the larger solvent accessible surface area of the 3_{10}-helical conformation (Table 6). The $\Delta E_{\text{uu-el}}$ stabilization of the 3_{10}-helix is greater in nonpolar solvents (Table 4). Since the ideal 3_{10}-helix would have one additional intrahelical hydrogen bond over the α-helix, this increase in the $\Delta E_{\text{uu-el}}$ term is a reflection of the better geometry of the 3_{10}-helical hydrogen bonds in nonpolar solvents (as seen in Table 2); this, of course, reflects the lack of competition with polar solvent. Thus, we have effectively stronger hydrogen bonds in low dielectric media. We have noted that as the polarity of the environment increases, a gradual widening of ψ occurs in the 3_{10}-helix as hydrogen bonding to the solvent increases. Thus, in polar environments, it is possible for the

(40) Huyghues-Despointes, B. M. P.; Scholtz, J. M.; Baldwin, R. L. *Protein Sci.* **1993**, *2*, 1604−1611.

Table 2. Mean Calculated Hydrogen-Bond Geometery[a] of Four Central Residues

	α-helix			3_{10}-helix		
	distance	donor	acceptor	distance	donor	acceptor
gas phase	2.1 ± 0.2	161.3 ± 9.8	153.4 ± 10	2.4 ± 0.5	156.9 ± 16.2	126.1 ± 12.4
CH_2Cl_2	2.1 ± 0.2	161.6 ± 9.7	153.1 ± 9.9	2.3 ± 0.3	158.2 ± 12.3	125.8 ± 11.7
CH_3CN	2.2 ± 0.3	159.0 ± 11.3	153.1± 11.2	2.6 ± 0.6	142.9 ± 22	116.8 ± 16.4
water	2.1 ± 0.2	162.0 ± 9.5	154.4± 10.2	2.7 ± 0.5	137.3± 22.7	113.3 ± 16.5

[a] Distance is the distance between the donor hydrogen and the acceptor oxygen. Donor is the donor angle made by atoms N- -H· ·O. Acceptor is the acceptor angle made by atoms H· ·O−C.

Table 3. Thermodynamic Data for the to α- to 3_{10}-Helical Transition

solvent	ΔA_{tot}	ΔE_{tot}	$-T\Delta S_{tot}$
in vacuo	3.2 ± 0.8	4.4 ± 1.2	−1.2 ± 0.4
CH_2Cl_2	5.8 ± 0.3	12 ± 2	−6 ± 2
CH_3CN	7.2 ± 0.2	10 ± 3	−3 ± 2
water	7.6 ± 0.4	12 ± 5	−4± 5

Table 4. Nonbonded Energetic Data for the α- to 3_{10}-Helix Transition in Various Environments

solvent	$\Delta E_{uu\text{-}vdw}$	$\Delta E_{uu\text{-}el}$	$\Delta_{Euv\text{-}vdw}$	$\Delta E_{uv\text{-}el}$
in vacuo	17.7 ± 1.3	−5.0 ± 2.1		
CH_2Cl_2	13.4 ± 0.6	−8.0 ± 1.6	−5.8 ± 0.9	10.1 ± 1.0
CH_3CN	10.3 ± 1.6	−3.5 ± 2.2	−5.1 ± 1	7.8 ± 2.2
water	6.7 ± 0.9	−0.1 ± 1.7	−1.4 ± 1.7	6 ± 7

Table 5. Average Dipole Moments of α- and 3_{10}-Helical States in Various Environments

	α-helix	3_{10}-helix
in vacuo	36.5 ± 1.4	30.6 ± 2.2
CH_2Cl_2	40.5 ± 0.8	34.0 ± 0.9
CH_3CN	39.2 ± 1.5	31.2 ± 1.4
water	34.8 ± 0.4	31.5 ± 1.6

Table 6. Average Surface Area of End Point Conformations in Each Simulation

	α−helix	3_{10}-helix
CH_2Cl_2	2466 ± 90	2685 ± 64
CH_3CN	2280 ± 161	2450 ± 241
water	2135 ± 181	2147 ± 239

peptide to reduce some of the inherent strain of the 3_{10}-helix (as shown in the $\Delta E_{uu\text{-}vdw}$ term) by widening ψ with the resulting weaker intrasolute hydrogen bonds being compensated by increased hydrogen bonding with the polar solvent. This effect is seen clearly in Figure 8.

The free-energy surfaces shown in Figure 1 illustrate that there is an observed activation barrier for the helical interconversion only in the gas phase. Indeed, the magnitude of the activation free energy for the conformational interconversion in the gas phase is 3.3 ± 0.2 kcal/mol from the α-helix and 0.1 ± 0.2 kcal/mol from the 3_{10}-helix. The barrier species is entropically stabilized ($-T\Delta S$) relative to the α-helix by 4.1 ± 0.5 kcal/mol and 7.4 ± 0.7 kcal/mol higher in potential energy. These data indicate an unfavorable energetic component of the barrier species, consistent with steric and or electrostatic clashes. If we break down the potential energy of the barrier species, we find that the unfavorable energy term is driven by the van der Waals term ($\Delta E_{uu\text{-}vdw}$ = 15.08 ± 1.75, $\Delta E_{uu\text{-}el}$ = −7.54 ± 4.70 kcal/mol). The barrier species is 3_{10}-helical-like as defined by averaging the conformations and hydrogen bond analysis. (The average distance between the central 3_{10} hydrogen-bond donors and acceptors is 2.3 ± 0.3 Å, with an average donor angle of 155.8 ± 15° and an acceptor angle of 124.9 ± 14°. Furthermore, the average torsion angles are $\phi = -56.0 \pm 10.8°$ and $\psi = -30.2 \pm 13.7°$. The total surface area of the transition state is 1344 ± 113 Å^2, slightly larger than the 3_{10}-helix.)

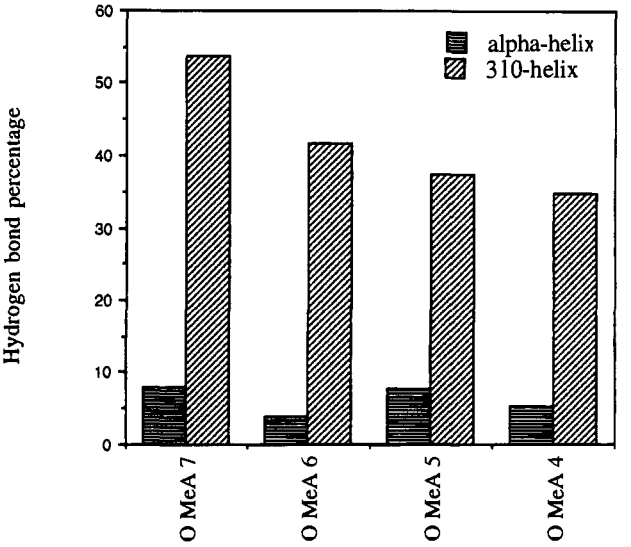

Figure 8. Percentage of hydrogen bonds made between the carbonyl oxygens and water in the α- and 3_{10}-helical conformation. Hydrogen bonds include bifurcated peptide to water hydrogen bonds and hydrogen bonds solely to water.

Discussion

The formation of either an α- or 3_{10}-helix for MeA-containing peptides arises from a subtle balance of many factors.[14] The interplay among these factors in guiding formation of an α- or 3_{10}-helix is not thoroughly understood. We have reported here pmfs for the α- to 3_{10}-helical transition of an MeA oligomer in order to elucidate the effect of the medium on the relative stability of the two helical forms and the transitions between them. MeA is a natural choice for this study given the possible mechanistic importance of α- to 3_{10}-helical transitions of peptaibols in ion-channel formation and the conformational properties of this residue.

Free-energy surfaces have been calculated for the transition in several environments (including water, CH_3CN, CH_2Cl_2, and vacuum). The free-energy surface of the gas phase simulation (Figure 1) illustrates that the α-helix and 3_{10}-helix occupy two distinct, fully-resolved wells on the free-energy surface with a minimal activation energy barrier between them. This should be contrasted with the case in solution. In fact, the lack of a transition barrier in solution indicates that, to the extent that our choice of reaction coordinate is a reasonable representation of the true conformational transition coordinate, the two helical forms occupy a single thermodynamic state. This helical state is essentially "molten" with any individual residue capable of hydrogen bonding to either the $i + 3$ or $i + 4$ with virtual energetic impunity (less than 1 kcal/mol). Peptide geometry would suggest an intermediate state, which allows a bifurcated hydrogen bond to both the $i + 3$ and $i + 4$ residues. This oscillation in hydrogen bond pattern has been reported by other

workers.[41,42] The polarity of the solvent as well as helical length (data not shown) has a pronounced effect on the shape of the single broad helical well. The pmf of the helical transition in CH_2Cl_2 is much flatter in the 3_{10}-helical region. That the helical end states do, in fact, conform to true and distinct α- and 3_{10}-conformations has been shown by the results of the detailed structural analysis presented.

From the thermodynamic data shown in Table 3, we conclude that, upon changing environments from gas phase to CH_2Cl_2 to CH_3CN or water, the α-helix becomes increasingly more stable than the 3_{10}-helix. The results indicate that the factors contributing to the stability of α-helices are more favorable solute−solvent electrostatic interactions (due to the additional exposed carbonyls and amides and greater dipole moment), more favorable intrasolute steric interactions, and more favorable intrasolute hydrogen-bonding geometries. This would tend to indicate that the lower-free-energy α-helical states in proteins would be those in which the termini of the helices are exposed to solvent, or in which the "matrix" of the protein (including the helical side chains) provides a suitable environment to "cap"[44,45] the termini of the helix and/or provide suitable residues to interact with the helix dipole. This is consistent with the vast amount of literature on the role of charged groups at the termini of helices[43,44] and the observed capping of protein helices.[45,46] The results also indicate that nonpolar environments stabilize 3_{10}-helices to a greater degree. This is due to the additional hydrogen bond of this conformation and the more favorable hydrogen-bonding geometry in nonpolar environments, leading to an effective increase in intrapeptide hydrogen bond strength.

These conclusions are consistent with experimental data that show MeA-containing peptides to be 3_{10}-helical in $CDCl_3$ and α-helical in $(CD)_3SO$.[47] In addition, the crystal structure of Boc-Trp-Ile-Ala-MeA-Ile-Val-MeA-Leu-MeA-Pro-OMe has been solved in several crystal forms with different co-crystallized solvents.[8] In one crystal, in which there are two co-crystallized water molecules,[48] the peptide is in an α-helical conformation. In another crystal,[49] which is anhydrous, the peptide is primarily a 3_{10}-type. The co-crystallized water molecules make hydrogen bond bridges between helical units and, along with the intermolecular peptide hydrogen bonds, satisfy most of the hydrogen-bonding requirement of the termini of the helix. For the anhydrous crystal, the termini of the 3_{10}-helix form several intermolecular hydrogen bonds between peptide units, but fewer than in the α-helical crystal. Similar analysis of the environment of peptide crystals by Otada *et al.*[50] has illustrated α-helical preference in polar media and 3_{10}-helical preference in nonpolar media, which is in agreement with our conclusions.

On the other hand, our results would not have predicted that a 16-residue, Ala-based peptide would be 3_{10}-helical in aqueous solution, as reported based on ESR spectroscopy.[51] This is particularly true since Clark *et al.*[16] concluded from their study that the α-helix of Ala-based peptides is more stable (in relation to the 3_{10}-helix) then MeA-containing peptides. We have recently synthesized similar Ala-based peptides containing a more conformationally constrained spin label[52] and, using similar ESR experiments, have determined that these peptides are α-helical,[53] in agreement with our calculations.

It has been shown that there is a length-dependent effect on the relative stability of α- and 3_{10}-helices.[13,50,54] The 3_{10}-helix predominates for shorter helical lengths, and the α-helix becomes increasingly favored with longer lengths. In the gas phase simulations of Huston and Marshall,[13] a conformational free-energy difference between the α- and 3_{10}-helix of an MeA nonomer was calculated as 1.1 kcal/mol. In comparison to the 3.3 kcal/mol of differential gas phase helical stability calculated here for a decamer of MeA, this implies a length-dependent effect of approximately 2.2 (kcal mol^{-1})/residue favoring the α-helix. One can estimate an equilibrium length *in vacuo* of approximately 7.5 residues where the two helical states would be approximately isoenergetic.

Previous estimates of the peptide length at which the two helical conformers of oligo-α-methylalanine are of roughly equal potential energy have been reported in the literature. This length has been calculated as 12 residues with the AMBER all-atom potential,[15] 8 residues with the AMBER united-atom potential,[17] 7 residues with AM1 semiempirical calculations,[55] and less than 7 residues with the AMBER/OPLS potential.[13] The effect of force field dependence on free energies is clearly seen in the case of blocked deca-α-methylalanine, for which the all-atom AMBER force field favors the 3_{10}-helix, while the AMBER united-atom and the AMBER/OPLS force fields favor the α-helix.[56] Given the enhanced α-helical stability of the alanine helices compared with α-methylalanine helices and the dramatic effect of solvation, with a solvent of high dielectric such as water enhancing this stability, it seems unlikely that isolated helices of moderate length derived from the α-monoalkylated residue would populate the 3_{10}-helical state significantly in the aqueous state.

Tirado-Rives *et al.*[24] have performed Monte Carlo calculations of the pmfs for the α- to 3_{10}-helical transition of blocked undecaalanine in the aqueous and gas phases. Despite the different peptides studied and some important differences in the reaction coordinates employed (see below), there are reasonable similarities between the two studies. Tirado-Rives *et al.*[24] observed that in the gas phase the 3_{10} minimum is shifted toward more positive values of ψ; our results display this same behavior (see Table 1). Corresponding to this is their observation that in water the carbonyl groups in the 3_{10} conformation were found to be more solvent exposed than in the α-helix, also consistent with the trends found here. The Monte Carlo study also found that solute−solute van der Waals energy contributes significantly to 3_{10} instability. This is consistent with the present results and with those previously reported.[14,15] Furthermore, we identify the solute−solvent electrostatic term as also contributing to the instability of the 3_{10}-helix. An unsettling discrepancy between the two studies is that Tirado-Rives *et al.*[24] find water to decrease the stability of the α-helix relative to the 3_{10}-helix, when compared to the conformational free-energy difference in vacuum. Our study illustrates the opposite trend; that is, the

(41) Soman, K. V.; Karimi, A.; Case, D. A. *Biopolymers* **1991**, *31*, 1351−1361.
(42) Sung, S.-S. *Biophys. J.* **1994**, *66*, 1796−1803.
(43) Hol, W. G. J. *Prog. Biophys. Mol. Biol* **1985**, *45*, 149−195.
(44) Hol, W. G. J. *Adv. Biophys.* **1985**, *19*, 133−165.
(45) Harper, E. T.; Rose, G. D. *Biochemistry* **1993**, *32*, 7605−7609.
(46) Presta, L. G.; Rose, G. D. *Science* **1988**, *240*, 1632−1641.
(47) Vijayakumar, E. K. S.; Balaram, P. *Biopolymers* **1983**, *22*, 2133−40.
(48) Karle, I. L.; Sukumar, M.; Balaram, P. *Proc. Natl. Acad. Sci. U.S.A.* **1986**, *83*, 9284−88.
(49) Karle, I. L.; Flippen, A. J. L.; Sukumar, M.; Balaram, P. *Int. J. Pept. Protein Res.* **1988**, *31*, 567−76.
(50) Otoda, K.; Yasuyuki, K.; Kimura, S.; Imanishi, Y. *Biopolymers* **1993**, *33*, 1337−1345.
(51) Miick, S. M.; Martinez, G. V.; Fiori, W. R.; Todd, A. P.; Millhauser, G. L. *Nature (London)* **1992**, *359*, 653−5.
(52) Marchetto, R.; Schreier, S.; Nakaie, C. R. *J. Am. Chem. Soc* **1993**, *115*, 11042−11043.
(53) Smythe, M. L.; Marshall, G. R. *J. Am. Chem. Soc.* Submitted for publication.
(54) Pavone, V.; Di, B. B.; Santini, A.; Benedetti, E.; Pedone, C.; Toniolo, C.; Crisma, M. *J. Mol. Biol.* **1990**, *214*, 633−5.
(55) Bindal, R. D.; Marshall, G. R. *J. Am. Chem. Soc.* Submitted for publication.
(56) Smythe, M. L.; Huston, S. E.; Marshall, G. R. in preparation.

effect of hydration is to increase the relative stability of the α-helix. In decamethylalanine, we have concluded that this is partly due to direct solute−solvent interactions, which are more favorable for the α-helical conformation.

It is worthwhile to discuss the different approaches taken in these two studies to define the conformational transition coordinate. The reaction coordinate employed by Tirado-Rives and co-workers was significantly different from that employed here; there the backbone ψ torsion angles were altered in tandem from those defining the 3_{10}-helix to those appropriate for an α-helix, and the ϕ torsion angles were held fixed at −60°. Therefore, only the bond angles and ω torsion angles were free to move, resulting in a much more restricted reaction coordinate than that used here. We note that the choice of reaction coordinate in the undecaalanine study was expedient, and perhaps necessary, due to the highly flexible nature of oligoalanine peptides. By contrast, the present decamethylalanine study benefits from previous, careful elucidation of the true reaction coordinate,[13] such that the arbitrary definition of a computationally expedient reaction coordinate was not necessary here. Furthermore, use of the unusual α,α-dialkylated amino acid, MeA, with its restricted conformational properties, in conjunction with the technique of umbrella sampling, allows calculation of the pmf without the use of any constraints on the peptide torsional degrees of freedom. (Of course, neither of these aspects of the current work, that is, the particular residue chosen for study nor the methodology employed, in itself obviates the use of guiding-constraints; it is their combination that is used to good advantage here.) The differences between the two studies give rise to quite different reaction pathways. For instance, the conformational transition pathway studies of Huston and Marshall[15] indicate that the changes in dihedral angle and hydrogen-bonding pattern along the reaction coordinate occur in a sequential fashion. This sequential character was noted previously in a study of oligoalanine conformational transition paths by Czerminski and Elber[26] and more recently in a molecular dynamics simulation of octamethylalanine.[23] Given the concerted nature of the pathway followed in the study of Tirado-Rives *et al.*,[24] two points should be made: First, the resulting free energy barrier should be regarded as an upper bound to the true activation free energy. And second, while the solvent response to the peptide motion along the defined reaction coordinate was included, the peptide-structural response to the presence of solvent was not. This is in contrast to the reaction coordinate used in the present simulations, which allows more complete inclusion of the peptide response to solvent environment.

One might question the relevance to proteins and peptides, which contain only mono-α-alkylated amino acids, of arguments derived from the study of MeA oligomers. Consider that MeA is a chimeric amino acid comprised of L- and D-Ala and that the presence of the *gem*-dimethyl groups should manifest themselves predominately through steric effects. The impact of such amino acids on peptide conformation is dramatic, as mentioned previously, and expected to increase the steric hinderance involved in conformational transitions, compared with transitions in, say, oligoalanine. Clearly, it may be concluded from the present study that even the, relatively crowded, peptide backbone of oligo-α-methylalanine allows the ready interchange of $[i,i+4]$ and $[i,i+3]$ hydrogen bonds. Therefore, the transition for α-monoalkylated peptides should be less sterically congested. Indeed, several recent MD simulations of α-monolkylated peptides[24,41,57] and proteins[58] have identified α- to 3_{10}-helical transitions.

Conclusion

The present study has addressed the solvation effects on the relative stability of the α- and 3_{10}-helices of decamethylalanine. It is clearly demonstrated by these calculations that aqueous conditions strongly favor the α-helix over the 3_{10}-helix. In addition, our results indicate that nonpolar environments, such as the interiors of proteins, membranes, and crystals could provide appropriate conditions for stabilizing the 3_{10}-helix. In these lower dielectric environments, the additional intramolecular hydrogen bond of the 3_{10}-helix results in an increase in 3_{10}-helix propensity. If one considers that the dielectric of CH_2Cl_2 at room temperature is 9.1, then one could argue that the transition from an α- to a 3_{10}-helix of an MeA decamer in lower dielectric environments would be less than in CH_2Cl_2 (6 kcal/mol). This is particularly important considering the observed preference of certain residues for either α- or 3_{10}-helices in proteins,[59] and the reported α- or 3_{10}-helical preference of peptides with identical amino acid composition but different sequences.[60,61] It is possible, therefore, that certain sequences of peptides may selectively form 3_{10}-helices based on side chain interactions, both intrahelical as seen with model peptides by Basu *et al.*[60,61] and between adjacent segments of the protein as implied by the longer 3_{10}-helices seen in proteins.[8] The relatively low activation energy barrier from the higher energetic state to the lower (less than 1 kcal/mol in these studies) for such transitions suggests that environmental changes could modulate the relative stability of the two helical forms in proteins and peptides and couple chemical to mechanical transformation at the molecular level. Such environmental changes could include the binding of substrates to proteins, or the addition of voltage across membranes, either of which might provide the free energy to trigger the α- to 3_{10}-helical transition. Furthermore, such facile interchange of local conformation may facilitate the transition from the molten globule to the compact state during protein folding. Thus, we contend that the α- to 3_{10}-helical transition may be a plausible mechanism in many such biological processes. The view of a cylindrical helix as a rod-like structure derived from crystal structures is clearly a static view; a relatively molten helix capable of easily optimizing its interactions and assisting in lowering the energetic barriers to conformational transitions is a much more appropriate characterization.

Acknowledgment. We thank Mr. R. Head for computational support and Drs. B. Ross and D. Pearlman for technical assistance with AMBER. This study was supported in part by grants from the National Institutes of Health (GM24483) and the Office of Naval Research (N00014-90-J-1393).

JA942833T

(57) Tirado-Rives, J.; Jorgensen, W. L. *Biochemistry* **1991**, *30*, 3864−3871.
(58) Fan, P.; Kominos, D.; Kitchen, D. B.; Levy, R. M.; Baum, J. *Chem. Phys.* **1991**, *158*, 295−301.
(59) Karpen, M. E.; De, H. P. L.; Neet, K. E. *Protein Sci.* **1992**, *1*, 1333−1342.
(60) Basu, G.; Bagchi, K.; Kuki, A. *Biopolymers* **1991**, *31*, 1763−1774.
(61) Basu, G.; Kuki, A. *Biopolymers* **1993**, *33*, 995−1000.